HHS Public Access

Author manuscript

Connect Tissue Res. Author manuscript; available in PMC 2022 November 01.

Published in final edited form as:

Connect Tissue Res. 2021 November ; 62(6): 698–708. doi:10.1080/03008207.2020.1865939.

Epiphyseal Cartilage Canal Architecture and Extracellular Matrix Remodeling in Mucopolysaccharidosis VII Dogs at the Onset of Postnatal Growth

Zhirui Jiang[1,2], **Casey P. Johnson**[3,4], **Olli Nykänen**[5], **Mikko Nissi**[5,6], **Yian Khai Lau**[1,2], **Meilun Wu**[1,2], **Margret L. Casal**[7], **Lachlan J. Smith**[1,2,*]

[1]Department of Neurosurgery, Perelman School of Medicine, University of Pennsylvania, Philadelphia, PA, USA

[2]Deparment of Orthopaedic Surgery, Perelman School of Medicine, University of Pennsylvania, Philadelphia, PA, USA

[3]Department of Veterinary Clinical Sciences, University of Minnesota, Saint Paul, MN, USA

[4]Center for Magnetic Resonance Research, University of Minnesota, Minneapolis, MN, USA

[5]Department of Applied Physics, University of Eastern Finland, Kuopio, Finland

[6]Department of Diagnostic Radiology, University of Oulu, Oulu, Finland

[7]Department of Clinical Sciences and Advanced Medicine, School of Veterinary Medicine, University of Pennsylvania, Philadelphia PA, USA

Abstract

Mucopolysaccharidosis VII is a genetic, lysosomal storage disease characterized by abnormal accumulation of glycosaminoglycans in cells and tissues. MPS VII patients exhibit multiple failures of endochondral ossification during postnatal growth, including markedly delayed cartilage-to-bone conversion in the vertebrae and long bones. Cartilage canals provide the template for vascularization at the onset of secondary ossification. The objective of this study was to investigate whether abnormal cartilage canal architecture and enzyme-mediated extracellular matrix (ECM) remodeling contribute to delayed cartilage-to-bone conversion in MPS VII. The epiphyseal cartilage canal networks of 9-day-old healthy control and MPS VII-affected dog vertebrae were characterized using high-resolution, contrast-free quantitative susceptibility mapping magnetic resonance imaging. Interestingly, the density, number, connectivity and

[*]**Correspondence:** Lachlan J. Smith, Ph.D., Associate Professor, Department of Neurosurgery, University of Pennsylvania, 371 Stemmler Hall, 3450 Hamilton Walk, Philadelphia, PA, 19104 USA, lachlans@pennmeducine.upenn.edu, Phone: +1 215 746 2169, Fax: +1 215 573 2133.

Author Contributions

ZJ contributed to conceptual design, performed experiments and drafted the manuscript; CPJ contributed to conceptual design, performed experiments and drafted the manuscript; ON and MN performed experiments; YKL and MW performed experiments; MLC cared for animals and contributed to conceptual design; and LJS contributed to conceptual design and drafted the manuscript. All authors reviewed and approved the manuscript prior to submission.

Data Availability Statement

Study data will be made available upon reasonable request to the corresponding author.

Disclosure Statement

The authors have nothing to disclose.

thickness of canals was not significantly different between MPS VII and control vertebrae. Immunohistochemistry revealed diminished MMP-9, but normal MMP-13 and 14 expression by epiphyseal cartilage chondrocytes, while active ALP and TRAP enzyme expression by chondrocytes and chondroclasts, respectively, were both diminished. Our findings suggest that while the epiphyseal cartilage canal network in MPS VII is normal at the onset of secondary ossification, expression of enzymes required for cartilage resorption and replacement with mineralized ECM, and initiation of angiogenesis, is impaired.

Keywords

Mucopolysaccharidosis; lysosomal storage disorder; magnetic resonance imaging; quantitative susceptibility mapping; canine; cartilage canals; endochondral ossification

Introduction

The mucopolysaccharidoses (MPS) are a family of inherited, lysosomal storage disorders characterized by deficient activity of enzymes that degrade glycosaminoglycans (GAGs).[1] These GAGs accumulate in cells and tissues leading to progressive cellular dysfunction.[1] MPS VII, also called Sly Syndrome, is characterized by deficient beta-glucuronidase activity, which results in accumulation of poorly degraded heparan, dermatan and chondroitin sulfate GAGs.[2] MPS VII patients exhibit severe skeletal abnormalities during postnatal growth, including dysplasia of the vertebrae and long bones, resulting in impaired mobility, and pain and paralysis that negatively impacts quality of life.[1] Previous studies in our lab using the naturally-occurring canine MPS VII model showed that the cartilage-to-bone conversion, a critical step during endochondral ossification, is markedly delayed in the secondary ossification centers (SOCs) of both vertebrae and long bones.[3–5] Similar observations have been reported in a mouse MPS VII model.[6, 7]

Formation of SOCs is a multi-stage process: chondrocytes first generate a cartilaginous template from mesenchymal condensations. At a certain point during postnatal growth, these chondrocytes exit the cell cycle and proceed through distinct stages of differentiation, including prehypertrophic, hypertrophic and terminal, before undergoing programmed death.[8] Cartilage canals spring from the periosteum and branch into the epiphyseal cartilage, providing a network for the invasion of blood vessels and osteoprogenitor cells to replace cartilage with bone.[9] Prior to undergoing apoptosis, chondrocytes secrete alkaline phosphatase (ALP) for initial mineralization of the cartilage extracellular matrix (ECM); this mineralized ECM is subsequently resorbed by multinucleated chondroclasts residing in cartilage canals.[10] Similar to osteoclasts, chondroclasts secrete tartrate-resistant acid phosphatase (TRAP) and enzymes including matrix metalloproteinases (MMPs) to mediate inorganic and organic ECM remodeling and resorption.[11] MMP-9 expressed by chondrocytes and chondroclasts degrades cartilaginous matrix and acts as an angiogenic factor by releasing vascular endothelial growth factor (VEGF) from the ECM.[12–14] MMP-13 and MMP-14 are also expressed by chondrocytes and chondroclasts to degrade ECM components including types I and II collagen, and aggrecan.[15–18] Meanwhile, blood vessels and osteoblasts invade through the cartilage canals[19–21] to drive formation of bone matrix.[8]

We previously showed that chondrocytes in MPS VII epiphyseal cartilage exhibit diminished hypertrophic differentiation capacity.[3, 5, 6] Our objectives in the current study were to build on this work and, firstly, establish whether abnormal cartilage canal network formation contributes to delayed SOC formation in MPS VII using high resolution contrast-free magnetic resonance imaging (MRI). Specifically, we applied a quantitative susceptibility mapping (QSM) MRI technique, which is sensitive to magnetic susceptibility differences between the canals and the surrounding epiphyseal cartilage,[22–25] to generate three-dimensional (3D) images of the cartilage canal networks in the vertebrae of MPS VII dogs at the onset of postnatal growth. Secondly, we used histological assays to assess impaired enzyme-mediated ECM resorption and mineralization in MPS VII vertebral epiphyseal cartilage.

Materials and methods

Animals and Tissue Collection

For these studies we used the naturally occurring MPS VII canine model. MPS VII dogs have a missense mutation (R166H) in the *GUSB* gene and exhibit a similar skeletal phenotype to human patients.[4, 26–28] All animal procedures were approved by the Institutional Animal Care and Use Committee of the University of Pennsylvania. Animals were raised and housed at the University of Pennsylvania School of Veterinary Medicine under NIH and USDA guidelines for the care and use of animals in research as previously described.[3] All animals were housed in the same facility (temperature-controlled kennel runs) and neonates were supplemented with Nurturall Puppy Milk Replacer (Veterinary Products Laboratories; Phoenix, US). Genotypes of control (heterozygous) and MPS VII (homozygous) dogs were determined via PCR analysis at birth. Animals (n=5 for both control and MPS VII; 10 animals total; 3 male and 2 female animals in both groups) were euthanized at 9 days-of-age via an overdose of sodium pentobarbital as previously described.[3] This age was selected as it immediately precedes commencement of vertebral secondary ossification in healthy animals. It is also the age immediately before delayed ossification firsts manifests in MPS VII dogs,[3] but where pathological changes at the molecular level are already evident.[5] All animals successfully reached the study end point and none were excluded from analyses. Sample sizes were selected based on prior work where n=5 was sufficient to detect significant differences between MPS VII and control (power > 0.90).[3, 5] Vertebral bodies (thoracic and lumbar) were isolated and either flash frozen and stored at −20 °C for subsequent MRI, or fixed in 10% neutral buffered formalin for histology, as outlined below.

MRI Analysis of Vertebral Epiphyseal Cartilage Canals

Isolated thoracic (T5 and T6) vertebrae from control and MPS VII animals were imaged at 9.4T MRI for assessment of epiphyseal cartilage canal network density and architecture. Prior to imaging, specimens were thawed and immersed in perfluoropolyether oil (Fomblin; Solvay Specialty Polymers; West Deptford, USA) to eliminate magnetic susceptibility artifacts at air-tissue interfaces. Specimens were then imaged using a preclinical 9.4T MRI scanner (Agilent Technologies; Santa Clara, USA) with a Varian console (Agilent) and an in-house saddle transmit/receive radiofrequency coil to acquire high-spatial-resolution,

magnetic susceptibility-weighted 3D gradient echo (GRE) images of epiphyseal cartilage canals, as previously described.[23, 29] Standard imaging parameters were: field-of view = 35 × 35 × 35 mm^3; sampling matrix = 384 × 384 × 384; acquired spatial resolution= 0.091 mm isotropic; TR/TE = 40/15.9 ms; flip angle =15°; bandwidth = 37 Hz/px; and scan time = 100 minutes.

The acquired susceptibility-weighted 3D GRE images were then processed to visualize epiphyseal cartilage canals. First, the epiphyseal cartilage regions were semi-automatically segmented using the 3D GRE magnitude images with ITK-SNAP (www.itksnap.org).[30] Second, a binary mask defined by these segmented regions was used for post-processing of the 3D GRE images using QSM to enhance the appearance of the cartilage canals, as previously described.[22, 31] Third, the visual appearance of the vessels was further refined using a Frangi vesselness filter to remove all structures that do not look like vessels.[32, 33] The QSM processing and Frangi vesselness filtering were performed in Matlab (R2019b; MathWorks; Natick, USA). 3D visualizations and maximum intensity projections of the cartilage canal images were generated using 3D slicer (www.slicer.org)[34] to illustrate the localization of cartilage canals in the epiphyseal cartilage.

Properties of the cartilage canals, including density, branching, number and thickness, were quantified. First, the cartilage canal density was calculated as the ratio of the total cartilage canal volume to epiphyseal cartilage volume in each of the segmented regions. For this calculation, cartilage canals were semi-automatically segmented based on the 3D QSM images using ITK-SNAP. Second, the cartilage canal segmentations were imported into image-analysis software using the package Imaging Processing Language (IPL; SCANCO Medical, Brüttisellen, Switzerland), and parameters including branching (connectivity), the number of cartilage canals, and cartilage canal overall thickness were then assessed. In addition to overall average thickness, thickness distribution was calculated by counting voxels within three increasing diameter ranges (0–0.091mm, 0.091–0.182mm and 0.182–0.273mm) and was visualized via heat maps.[35, 36]

Immunohistochemistry

To assess relative protein expression of MMPs, lumbar vertebral bodies (L1) were fixed in 10% neutral buffered formalin for 1–2 weeks and then decalcified (Formical 2000; Statlab; McKinney, USA) prior to paraffin processing and embedding. Immunohistochemistry was carried out on 5 μm sections after deparaffinization. Antigen retrieval was carried out by incubating sections with 2 mg/mL hyaluronidase and 0.1 U/mL chondroitinase ABC at 37°C for 30 min. Sections were then treated with 3% hydrogen peroxide for 12 minutes to block endogenous peroxidase activity, followed by Background Buster (Innovex Biosciences; Richmond, USA) for 10 minutes at room temperature to block non-specific protein binding. Sections were then incubated with the following primary antibodies and concentrations: MMP-9 (ab38898, 1:400; Abcam, USA), MMP-13 (ab39012, 1:400; Abcam) and MMP-14 (ab51074, 1:400; Abcam) overnight at 4°C. Antibody staining was visualized using the Vectastain Elite ABC-Peroxidase Kit (Vector Laboratories; Burlingame, USA) and diaminobenzidine chromogen (Thermofisher Scientific; Waltham, USA) according to the manufacturer's protocols. Sections were counterstained with hematoxylin. For analysis, all

slides were imaged under bright field light microscopy (Eclipse 90i; Nikon; Tokyo, Japan). Three randomly selected regions of interest within the epiphyseal cartilage were analyzed. For each region, the number of immunopositive cells was counted and normalized as a percentage of the total number of cells present. Cell counting for each region was performed by three individuals who were blinded to the study groups and averaged. The average result for all three regions measured by the three individuals was then determined and taken as a single biological replicate for statistical comparisons. Negative isotype controls for these antibodies were published previously.[37]

In Situ ALP and TRAP Enzyme Staining

To assess relative ALP and TRAP enzyme staining in epiphyseal cartilage, thoracic vertebral bodies (T7 and T8) were fixed in 10% neutral buffered formalin overnight and then in placed in 30% sucrose prior to embedding in OCT compound. Five μm-thick, mid-sagittal, calcified cryosections were cut using the Kawamoto film method (Section-Lab Co. Ltd.; Hiroshima, Japan).[38] Either ALP or TRAP staining was performed (MK300, Takara Bio Inc.; Kasatsu, Japan) following the manufacturer's instructions. The number of TRAP-positive chondroclasts per cartilage canal, as well as the total number of cartilage canals present, were quantified.

Statistics

Statistical analyses were performed using GraphPad Prism version 8.0 (GraphPad Software Inc.; California, USA). Data were tested for normality using Q-Q plots, and significant differences between control and MPS VII for each experimental outcome were established using Mann-Whitney U tests. Results were reported as median and interquartile range. Statistical significance was defined as $p<0.05$.

Results

MRI Analysis of Vertebral Epiphyseal Cartilage Canals

We successfully applied QSM MRI to generate detailed 3D renderings of vertebral epiphyseal cartilage canal network architecture in control and MPS VII dogs. Axial, maximum intensity projections through the complete thickness of epiphyseal cartilage at the cranial end of T6 vertebrae from each control and MPS VII animal (Figures 1A and B) showed cartilage canals originating from the perichondrium at the vertebral periphery and radiating inwards towards the center of the epiphyses. Quantitative analyses comparing architectural parameters of cartilage canal between control and MPS VII vertebrae were initially performed separately for cranial and caudal epiphyseal cartilage (average of T5 and T6 vertebrae), as well as the combined average of these two regions. Images illustrated a high degree of within-group sample-sample variability, and median cartilage canal density was found to be similar between control (5.2%, IQR=4.7–5.3%) and MPS VII (4.8%, IQR=4.5–4.8%) dog vertebrae (Figure 1C, $p=0.98$). Furthermore, cartilage canal branching and number were also not significantly different between control and MPS VII dogs (Figure 1D and E). Heat maps were used to illustrate cartilage canal thickness distribution in the vertebral epiphyseal cartilage (Figures 2A and B). There were no significant differences in

the overall average thickness of cartilage canals, or thickness distribution within the three diameter ranges analyzed, between control and MPS VII dogs (Figures 2C–F).

Histological Assessment of Epiphyseal Cartilage Remodeling

Matrix metalloproteinases MMP-9, MMP-13 and MMP-14 mediate remodeling of cartilage, while MMP-9 is also an angiogenic factor. With respect to MMP-9, in epiphyseal cartilage from control dog vertebrae there was positive immunostaining observed both in the ECM and by resident chondrocytes (Figure 3A). In contrast, in epiphyseal cartilage from MPS VII vertebrae, both ECM and cell-associated MMP-9 staining was markedly lower (Figure 3A). Quantitative analysis revealed the number of MMP-9 positive chondrocytes was 28% percent lower in MPS VII vs control epiphyseal cartilage (median of 10.7%, IQR = 10.5–16.5%, vs median of 43.5%, IQR =27.4–56.6%, of total cells, respectively; p=0.032; Figure 3B). In contrast, immunostaining for MMP-13 and MMP-14 revealed similar expression levels in control and MPS VII epiphyseal cartilage for both these molecules, which was confirmed through quantitative assessments of the relative numbers of immunopositive cells (Figures 3C–F).

With respect to active ALP enzyme expression, there was positive, punctate staining associated with chondrocytes in the epiphyseal cartilage of control vertebrae; however, ALP staining was completely absent in MPS VII cartilage (Figure 4A). Finally, the number of TRAP-positive chondroclasts per cartilage canal was found to be significantly lower in MPS VII vertebral epiphyseal cartilage compared to controls (median of 0.3, IQR = 0–0.3, vs median of 3.7, IQR = 3.4–3.7), respectively; p = 0.008; Figures 4B and C). Similar to MRI findings (Figure 1), histological analysis also found there was no significant difference in the number of cartilage canals in the epiphyses between control and MPS VII dogs (Figure 4D).

Discussion

Vascularization, epiphyseal chondrocyte hypertrophy and ECM remodeling are all critical for effective cartilage-to-bone conversion during the process of endochondral ossification. In previous work we demonstrated that failed cartilage-to-bone conversion in canine MPS VII vertebral SOCs is in part due to the diminished capacity of resident chondrocytes to undergo hypertrophic differentiation, which is in turn associated with impaired activation of osteogenic signaling, including elements of the BMP and Wnt/β-catenin pathways.[3, 5] In this study, we aimed to build on these findings and investigate whether epiphyseal cartilage vascularization and ECM remodeling are also impaired. We demonstrated that QSM MRI can be applied to visualize canals in the epiphyseal cartilage of developing canine vertebrae. We were able to successfully use these QSM images to quantify key architectural characteristics of cartilage canals including density, number, branching and thickness. Our findings suggest that early in postnatal growth, cartilage canal architecture in vertebral epiphyseal cartilage is not significantly different between MPS VII and controls dogs; however, immunohistochemistry and in situ active enzyme staining revealed diminished expression of enzymes related to ECM degradation, mineralization and angiogenesis in MPS VII, which likely contributes to impaired cartilage-to-bone conversion.

Formation of cartilage canals in humans, and animals such as dogs and rabbits, takes place during embryonic development, providing a network for blood vessel in-growth, and nutrient and waste exchange.[9, 39] Although our findings showed normal cartilage canal network architecture in MPS VII vertebrae, this may not necessarily reflect normal vascularity. Cartilage canals are comprised of both connective tissue and blood vessels, as well as multinucleated chondroclasts present in vessel walls.[40] The source of QSM contrast to visualize cartilage canals includes remnants of blood, which increase susceptibility values; however, mineralization and the canal structure itself may also lead to positive QSM contrast. Thus, the QSM MRI technique visualizing cartilage canals may not provide definitive information on the presence and integrity of blood vessels within those canals, which is a prerequisite for delivery of osteoprogenitor cells and other factors required for the initiation of ossification.[40, 41] In future studies, perfusion of radio-opaque contrast agents in combination with microCT imaging may allow explicit visualization of blood vessels in the cartilage canals of MPS VII vertebral epiphyses.[42]

Chondroclasts are osteoclast-like, multinucleated cells that reside in cartilage canals, which function to degrade cartilage but not bone.[10, 11] Although relatively little is known about the origin of these chondroclasts, it is possible that their reduced numbers in MPS VII is attributed to impaired delivery through blood vessels. The exact function of the TRAP enzyme expressed by chondroclasts in cartilage canals with respect to ECM degradation is not clear; however, TRAP-deficient mice do exhibit disrupted formation of SOCs.[43] Decreased numbers of TRAP-expressing chondroclasts in MPS VII cartilage canals may reflect diminished ECM remodeling capacity at the onset of secondary ossification.

In recent studies we reported the presence of storage vacuoles containing accumulated GAGs in most skeletal cell types, including epiphyseal chondrocytes, in the vertebrae of 9-day-old MPS VII dogs,[37] and that this storage is associated with aberrant expression of molecules involved in endochondral ossification.[5] Expressed by both, epiphyseal chondrocytes and chondroclasts, MMPs −9, −13 and −14 are essential for ECM remodeling at multiple phases of SOC formation, including cartilage canal formation, vascular recruitment, and replacement of cartilaginous ECM with mineralized bone.[10, 11, 15–17, 44, 45] We found previously that both MMP-9 and −13 mRNA expression levels were significantly lower in MPS VII dog vertebral epiphyseal cartilage at 9 days-of-age, while MMP-14 expression was not significantly different.[5] Another study reported significantly lower MMP-13 mRNA expression levels in growth plates of 3-week-old MPS VII mice.[46] Here, examining chondrocyte-associated protein expression in 9-day-old dogs, we found that only MMP-9 was significantly lower in MPS VII, while MMPs −13 and −14 were not significantly different from controls. One possible explanation for the discrepancy between the bulk mRNA expression findings of the prior canine study,[5] and cell-associated protein expression in the current study is that bulk mRNA represents all cells present, not just epiphyseal chondrocytes. Further, it is likely that changes in protein expression lag changes in mRNA expression, as MMPs are upregulated during the earliest stages of cartilage-to-bone conversion. Future studies will further examine dynamic changes in MMP protein expression by examining animals at older ages. MMP-9 (or gelatinase B) both degrades components of the ECM and regulates the release of ECM-bound VEGF, making it a key mediator of angiogenesis.[12–14] The lower numbers of MMP-9-positive chondrocytes

observed in MPS VII vertebral epiphyseal cartilage and may indicate that although the architecture of cartilage canals was not significantly altered, vessel formation within those canals may be impaired.

Whether bone deposition during ossification is mediated by invasion of osteoblasts or, potentially, by trans-differentiation of hypertrophic chondrocytes to osteoblasts,[47] formation of the SOCs is initiated by mineralization of the cartilaginous ECM. Secretion of ALP by hypertrophic chondrocytes is a prerequisite for ECM mineralization. Although SOC formation has not initiated in either control or MPS VII vertebral epiphyses at 9 days-of-age,[3] the presence of ALP expression in controls indicates initiation of ECM mineralization. Furthermore, the absence of ALP expression in MPS VII dog vertebral epiphyses likely reflects the diminished mineralization capacity of MPS VII epiphyseal chondrocytes. In our recent study, significantly elevated lysosomal storage was described in MPS VII epiphyseal chondrocytes at 9 days-of-age, which was in turn associated with impaired autophagy and elevated apoptosis.[37] Cellular dysregulation resulting from this storage also likely contributes to diminished ALP expression and mineralizing capacity by these cells.

To our knowledge, this is the first study to utilize QSM-MRI to visualize cartilage canals in MPS animals. There were several limitations. As outlined above, this technique is not able to distinguish conclusively between cartilage canals that contain blood vessels and those that do not. Further, it is possible that very small canals are below the detectable limit of QSM MRI,[23] potentially masking any differences. As QSM MRI has been applied successfully in previous studies to detect cartilage canals in comparable tissues,[22–25] we believe that the failure to find significant differences in the current study is most likely due to the small effect size, rather than inadequacies of the imaging technique. The fact that complementary histological analysis also found no difference in cartilage canal numbers between groups supports this conclusion. Another limitation was that we only examined samples from dogs at a single age (9-days), and cartilage canal formation is a dynamic process. Additionally, we also only examined samples from a single skeletal site (the vertebrae), and it is possible that cartilage canal formation progresses differently at other sites such as in the SOCs of long bones. Also, MRI and histological analyses were performed at different spinal levels. Although delayed development of SOCs has been observed in both thoracic and lumbar vertebrae in MPS VII dogs, it is possible that findings could vary across spinal levels.

In conclusion, in this study we found that the vertebrae of MPS VII dogs exhibit normal epiphyseal cartilage canal architecture at the onset of postnatal growth; however, reduced numbers of TRAP-expression chondroclasts, and diminished MMP-9 and ALP expression by epiphyseal chondrocytes suggest that blood vessel formation, ECM remodeling and mineralization are impaired. Ongoing studies will seek to establish the molecular mechanisms linking GAG accumulation, abnormal vascularization, ECM remodeling and failed bone formation in MPS, with the long-term goal of developing improved therapies for skeletal disease in MPS patients.

Acknowledgements

Funding for this work was received from the National Institutes of Health (R01AR071975 and K01AR070894), the National MPS Society and WM Keck Foundation. Additional support received from the Penn Center for

Musculoskeletal Disorders Histology and MicroCT Cores (NIH P30AR069619). Animal care provided by staff at the Penn Referral Center for Animal Models (NIH P40OD010939) is gratefully acknowledged. Special thanks to Dr. Kai D. Ludwig for providing the Frangi filtering code.

References

1. Neufeld E, Muenzer J. The mucopolysaccharidoses. In: Sciver C, Beaudet A, Sly W and Valle D editors. The mucopolysaccharidoses. The metabolic and molecular bases of inherited disease; New York: McGraw hill; 2001.
2. Sly WS, Quinton BA, McAlister WH, Rimoin DL. Beta glucuronidase deficiency: Report of clinical, radiologic, and biochemical features of a new mucopolysaccharidosis. J Pediatr 1973;82(2): 249–257. [PubMed: 4265197]
3. Peck SH, O'Donnell PJM, Kang JL, Malhotra NR, Dodge GR, Pacifici M, Shore EM, Haskins ME, Smith LJ. Delayed hypertrophic differentiation of epiphyseal chondrocytes contributes to failed secondary ossification in mucopolysaccharidosis vii dogs. Molecular Genetics and Metabolism 2015;116(3): 195–203. [PubMed: 26422116]
4. Smith LJ, Martin JT, Szczesny SE, Ponder KP, Haskins ME, Elliott DM. Altered lumbar spine structure, biochemistry, and biomechanical properties in a canine model of mucopolysaccharidosis type vii. J Orthop Res 2010;28(5): 616–622. [PubMed: 19918911]
5. Peck SH, Tobias JW, Shore EM, Malhotra NR, Haskins ME, Casal ML, Smith LJ. Molecular profiling of failed endochondral ossification in mucopolysaccharidosis vii. Bone 2019;128(115042. [PubMed: 31442675]
6. Jiang Z, Derrick-Roberts ALK, Jackson MR, Rossouw C, Pyragius CE, Xian C, Fletcher J, Byers S. Delayed development of ossification centers in the tibia of prenatal and early postnatal mps vii mice. Mol Genet Metab 2018;124(2): 135–142. [PubMed: 29747998]
7. Jiang Z, Derrick-Roberts ALK, Reichstein C, Byers S. Cell cycle progression is disrupted in murine mps vii growth plate leading to reduced chondrocyte proliferation and transition to hypertrophy. Bone 2020;132(115195. [PubMed: 31863960]
8. Mackie EJ, Ahmed YA, Tatarczuch L, Chen KS, Mirams M. Endochondral ossification: How cartilage is converted into bone in the developing skeleton. Int J Biochem Cell Biol 2008;40(1): 46–62. [PubMed: 17659995]
9. Blumer MJ, Longato S, Richter E, Perez MT, Konakci KZ, Fritsch H. The role of cartilage canals in endochondral and perichondral bone formation: Are there similarities between these two processes? J Anat 2005;206(4): 359–372. [PubMed: 15817104]
10. Odgren PR, Witwicka H, Reyes-Gutierrez P. The cast of clasts: Catabolism and vascular invasion during bone growth, repair, and disease by osteoclasts, chondroclasts, and septoclasts. Connective tissue research 2016;57(3): 161–174. [PubMed: 26818783]
11. Blumer MJF, Longato S, Fritsch H. Localization of tartrate-resistant acid phosphatase (trap), membrane type-1 matrix metalloproteinases (mt1-mmp) and macrophages during early endochondral bone formation. Journal of anatomy 2008;213(4): 431–441. [PubMed: 18643874]
12. Engsig MT, Chen QJ, Vu TH, Pedersen AC, Therkidsen B, Lund LR, Henriksen K, Lenhard T, Foged NT, Werb Z et al. Matrix metalloproteinase 9 and vascular endothelial growth factor are essential for osteoclast recruitment into developing long bones. J Cell Biol 2000;151(4): 879–889. [PubMed: 11076971]
13. Vu TH, Shipley JM, Bergers G, Berger JE, Helms JA, Hanahan D, Shapiro SD, Senior RM, Werb Z. Mmp-9/gelatinase b is a key regulator of growth plate angiogenesis and apoptosis of hypertrophic chondrocytes. Cell 1998;93(3): 411–422. [PubMed: 9590175]
14. Hawinkels LJ, Zuidwijk K, Verspaget HW, de Jonge-Muller ES, van Duijn W, Ferreira V, Fontijn RD, David G, Hommes DW, Lamers CB et al. Vegf release by mmp-9 mediated heparan sulphate cleavage induces colorectal cancer angiogenesis. Eur J Cancer 2008;44(13): 1904–1913. [PubMed: 18691882]
15. Sakakura Y, Hosokawa Y, Tsuruga E, Irie K, Nakamura M, Yajima T. Contributions of matrix metalloproteinases toward meckel's cartilage resorption in mice: Immunohistochemical studies, including comparisons with developing endochondral bones. Cell and Tissue Research 2007;328(1): 137–151. [PubMed: 17136358]

16. Inada M, Wang Y, Byrne MH, Rahman MU, Miyaura C, López-Otín C, Krane SM. Critical roles for collagenase-3 (mmp13) in development of growth plate cartilage and in endochondral ossification. Proceedings of the National Academy of Sciences of the United States of America 2004;101(49): 17192–17197. [PubMed: 15563592]
17. Holmbeck K, Bianco P, Caterina J, Yamada S, Kromer M, Kuznetsov SA, Mankani M, Robey PG, Poole AR, Pidoux I et al. Mt1-mmp-deficient mice develop dwarfism, osteopenia, arthritis, and connective tissue disease due to inadequate collagen turnover. Cell 1999;99(1): 81–92. [PubMed: 10520996]
18. Mitchell PG, Magna HA, Reeves LM, Lopresti-Morrow LL, Yocum SA, Rosner PJ, Geoghegan KF, Hambor JE. Cloning, expression, and type ii collagenolytic activity of matrix metalloproteinase-13 from human osteoarthritic cartilage. J Clin Invest 1996;97(3): 761–768. [PubMed: 8609233]
19. Carlevaro MF, Cermelli S, Cancedda R, Descalzi Cancedda F. Vascular endothelial growth factor (vegf) in cartilage neovascularization and chondrocyte differentiation: Auto-paracrine role during endochondral bone formation. Journal of Cell Science 2000;113(1): 59–69. [PubMed: 10591625]
20. Burkus JK, Ganey TM, Ogden JA. Development of the cartilage canals and the secondary center of ossification in the distal chondroepiphysis of the prenatal human femur. The Yale Journal of Biology and Medicine 1993;66(3): 193–202. [PubMed: 8209555]
21. Maes C, Stockmans I, Moermans K, Van Looveren R, Smets N, Carmeliet P, Bouillon R, Carmeliet G. Soluble vegf isoforms are essential for establishing epiphyseal vascularization and regulating chondrocyte development and survival. J Clin Invest 2004;113(2): 188–199. [PubMed: 14722611]
22. Nissi MJ, Toth F, Wang L, Carlson CS, Ellermann JM. Improved visualization of cartilage canals using quantitative susceptibility mapping. PLoS One 2015;10(7): e0132167. [PubMed: 26168296]
23. Nissi MJ, Toth F, Zhang J, Schmitter S, Benson M, Carlson CS, Ellermann JM. Susceptibility weighted imaging of cartilage canals in porcine epiphyseal growth cartilage ex vivo and in vivo. Magn Reson Med 2014;71(6): 2197–2205. [PubMed: 23857631]
24. Wang L, Nissi MJ, Toth F, Johnson CP, Garwood M, Carlson CS, Ellermann J. Quantitative susceptibility mapping detects abnormalities in cartilage canals in a goat model of preclinical osteochondritis dissecans. Magnetic Resonance in Medicine 2017;77(3): 1276–1283. [PubMed: 27018370]
25. Johnson CP, Wang L, Toth F, Aruwajoye O, Kirkham B, Carlson CS, Kim HKW, Ellermann JM. Quantitative susceptibility mapping detects neovascularization of the epiphyseal cartilage after ischemic injury in a piglet model of legg-calve-perthes disease. J Magn Reson Imaging 2019;50(1): 106–113. [PubMed: 30556613]
26. Haskins ME. Animal models for mucopolysaccharidosis disorders and their clinical relevance. Acta Paediatr Suppl 2007;96(455): 56–62.
27. Haskins ME, Desnick RJ, DiFerrante N, Jezyk PF, Patterson DF. Beta-glucuronidase deficiency in a dog: A model of human mucopolysaccharidosis vii. Pediatr Res 1984;18(10): 980–984. [PubMed: 6436780]
28. Ray J, Bouvet A, DeSanto C, Fyfe JC, Xu D, Wolfe JH, Aguirre GD, Patterson DF, Haskins ME, Henthorn PS. Cloning of the canine beta-glucuronidase cdna, mutation identification in canine mps vii, and retroviral vector-mediated correction of mps vii cells. Genomics 1998;48(2): 248–253. [PubMed: 9521879]
29. Toth F, Nissi MJ, Zhang J, Benson M, Schmitter S, Ellermann JM, Carlson CS. Histological confirmation and biological significance of cartilage canals demonstrated using high field mri in swine at predilection sites of osteochondrosis. J Orthop Res 2013;31(12): 2006–2012. [PubMed: 23939946]
30. Yushkevich PA, Piven J, Hazlett HC, Smith RG, Ho S, Gee JC, Gerig G. User-guided 3d active contour segmentation of anatomical structures: Significantly improved efficiency and reliability. NeuroImage 2006;31(3): 1116–1128. [PubMed: 16545965]
31. Tóth F, Johnson CP, Mills B, Nissi MJ, Nykänen O, Ellermann J, Ludwig KD, Tompkins M, Carlson CS. Evaluation of the suitability of miniature pigs as an animal model of juvenile osteochondritis dissecans. Journal of Orthopaedic Research® 2019;37(10): 2130–2137. [PubMed: 31115932]

32. Wells WM, Colchester A and Delp S editors. Multiscale vessel enhancement filtering. First International Conference on Medical Image Computing and Computer-Assisted Intervention; October 11–13; Cambridge, MA, USA; date. 130–137.
33. Ellermann JM, Ludwig KD, Nissi MJ, Johnson CP, Strupp JP, Wang L, Zbyn S, Toth F, Arendt E, Tompkins M et al. Three-dimensional quantitative magnetic resonance imaging of epiphyseal cartilage vascularity using vessel image features: New insights into juvenile osteochondritis dissecans. JB JS Open Access 2019;4(4).
34. Fedorov A, Beichel R, Kalpathy-Cramer J, Finet J, Fillion-Robin JC, Pujol S, Bauer C, Jennings D, Fennessy F, Sonka M et al. 3d slicer as an image computing platform for the quantitative imaging network. Magn Reson Imaging 2012;30(9): 1323–1341. [PubMed: 22770690]
35. Downey CM, Singla AK, Villemaire ML, Buie HR, Boyd SK, Jirik FR. Quantitative ex-vivo micro-computed tomographic imaging of blood vessels and necrotic regions within tumors. PLOS ONE 2012;7(7): e41685. [PubMed: 22848565]
36. Nebuloni L, Kuhn GA, Vogel J, Müller R. A novel in vivo vascular imaging approach for hierarchical quantification of vasculature using contrast enhanced micro-computed tomography. PloS one 2014;9(1): e86562–e86562. [PubMed: 24475146]
37. Jiang Z, Lau YK, Wu M, Casal ML, Smith LJ. Ultrastructural analysis of different skeletal cell types in mucopolysaccharidosis dogs at the onset of postnatal growth. J Anat 2020.
38. Kawamoto T, Kawamoto K. Preparation of thin frozen sections from nonfixed and undecalcified hard tissues using kawamot's film method (2012). Methods Mol Biol 2014;1130(149–164. [PubMed: 24482171]
39. Haines RW. Cartilage canals. Journal of anatomy 1933;68(Pt 1): 45–64. [PubMed: 17104463]
40. Kugler JH, Tomlinson A, Wagstaff A, Ward SM. The role of cartilage canals in the formation of secondary centres of ossification. J Anat 1979;129(Pt 3): 493–506. [PubMed: 541238]
41. Liu S, Brisset JC, Hu J, Haacke EM, Ge Y. Susceptibility weighted imaging and quantitative susceptibility mapping of the cerebral vasculature using ferumoxytol. J Magn Reson Imaging 2018;47(3): 621–633. [PubMed: 28731570]
42. Nyangoga H, Mercier P, Libouban H, Baslé MF, Chappard D. Three-dimensional characterization of the vascular bed in bone metastasis of the rat by microcomputed tomography (microct). PloS one 2011;6(3): e17336–e17336. [PubMed: 21464932]
43. Hayman AR, Jones SJ, Boyde A, Foster D, Colledge WH, Carlton MB, Evans MJ, Cox TM. Mice lacking tartrate-resistant acid phosphatase (acp 5) have disrupted endochondral ossification and mild osteopetrosis. Development 1996;122(10): 3151–3162. [PubMed: 8898228]
44. Paiva KB, Granjeiro JM. Bone tissue remodeling and development: Focus on matrix metalloproteinase functions. Arch Biochem Biophys 2014;561(74–87. [PubMed: 25157440]
45. Davoli MA, Lamplugh L, Beauchemin A, Chan K, Mordier S, Mort JS, Murphy G, Docherty AJ, Leblond CP, Lee ER. Enzymes active in the areas undergoing cartilage resorption during the development of the secondary ossification center in the tibiae of rats aged 0–21 days: Ii. Two proteinases, gelatinase b and collagenase-3, are implicated in the lysis of collagen fibrils. Dev Dyn 2001;222(1): 71–88. [PubMed: 11507770]
46. Metcalf JA, Zhang Y, Hilton MJ, Long F, Ponder KP. Mechanism of shortened bones in mucopolysaccharidosis vii. Mol Genet Metab 2009;97(3): 202–211. [PubMed: 19375967]
47. Aghajanian P, Mohan S. The art of building bone: Emerging role of chondrocyte-to-osteoblast transdifferentiation in endochondral ossification. Bone Research 2018;6(1): 19. [PubMed: 29928541]

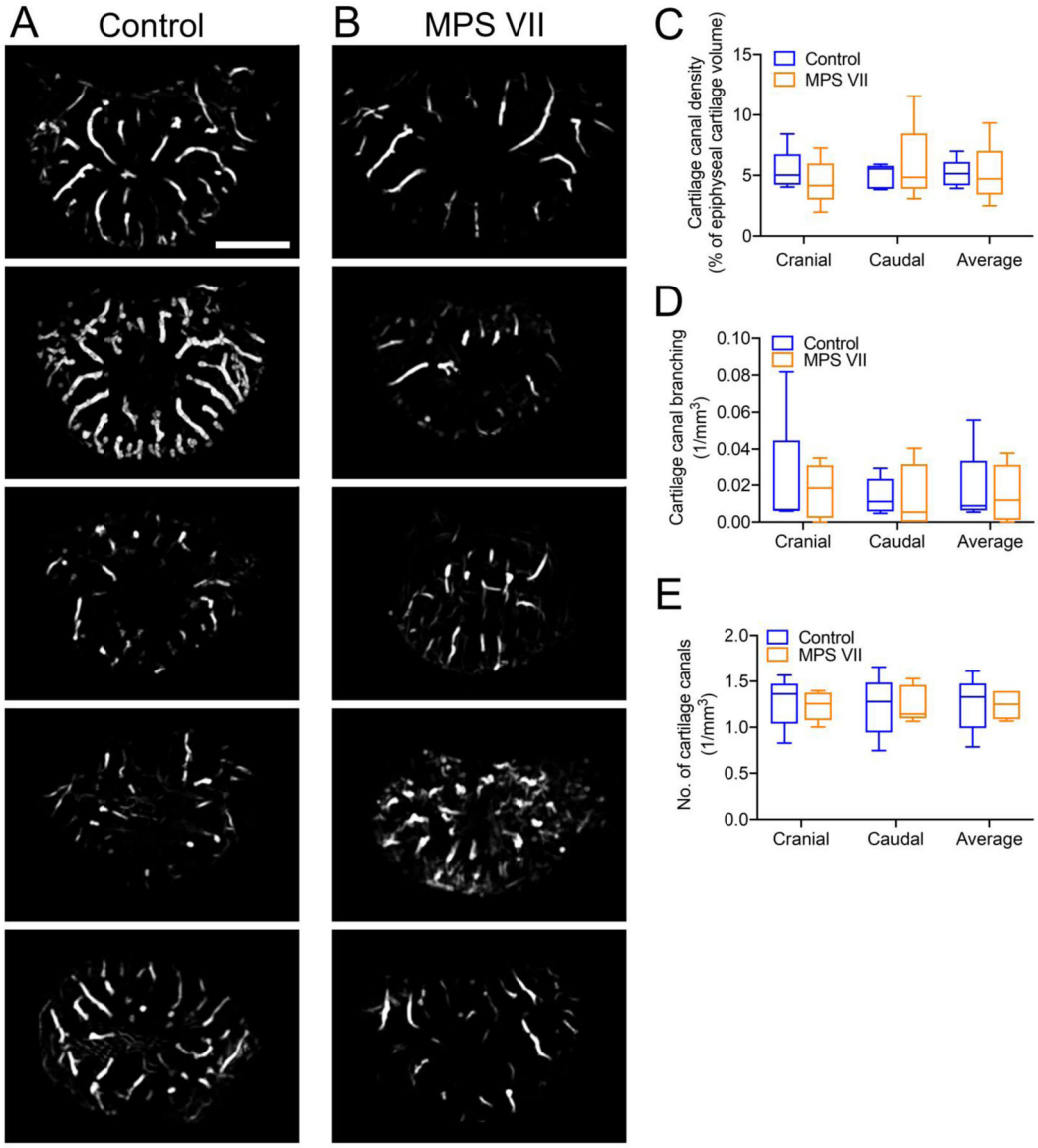

Figure 1. Cartilage canal architecture in vertebral epiphyseal cartilage.

QSM-MRI images showing cartilage canals in the cranial vertebral epiphyseal cartilage of: **A**. Five control (heterozygous) and **B**. Five MPS VII dogs (axial, maximum intensity projections). Quantification of **C**. Cartilage canal density; **D**. Cartilage canal branching; and **E**. Number of cartilage canals. N = 5; bar = 2 mm; median, interquartile range (box), and 10th and 90th percentiles (whiskers).

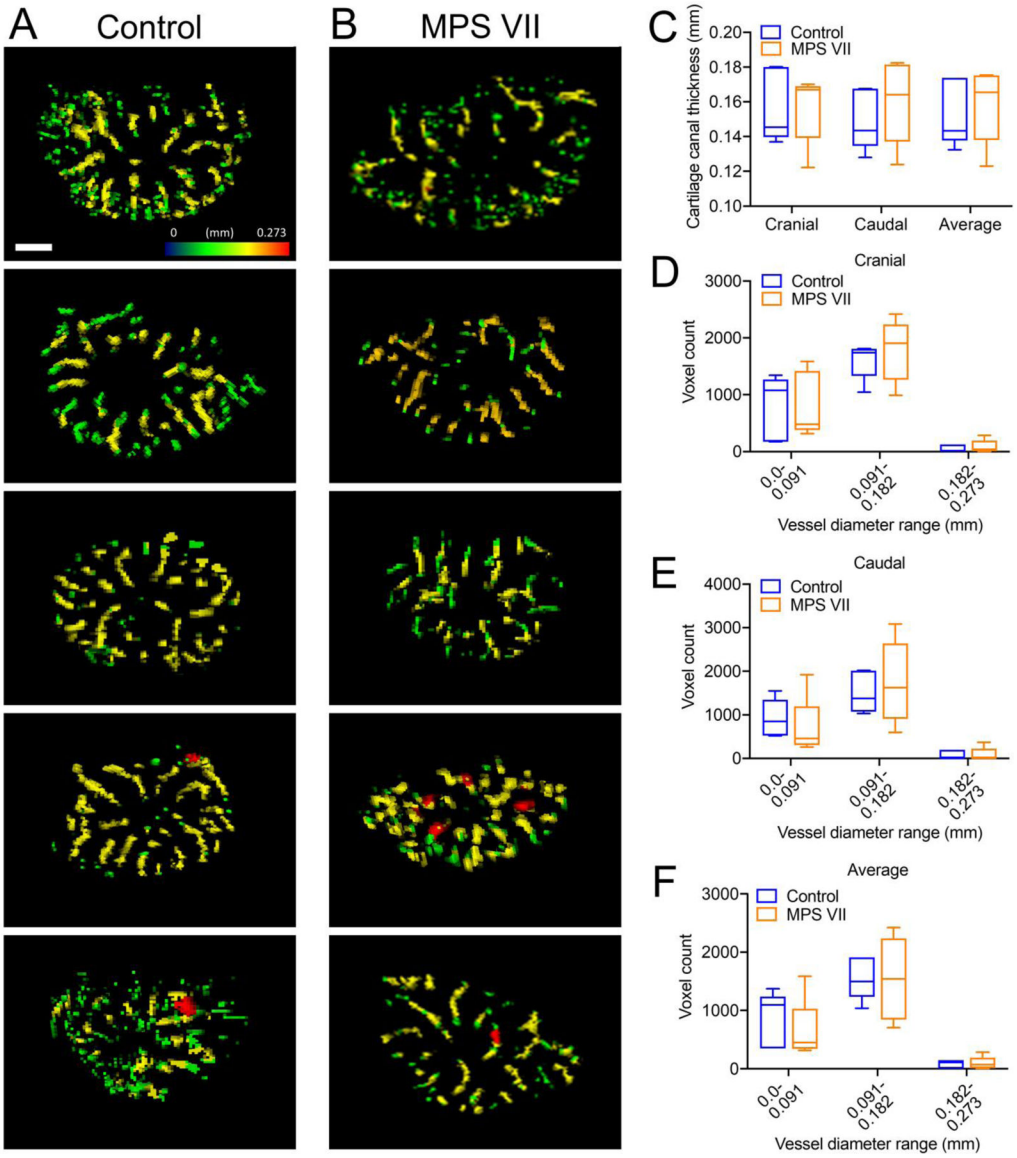

Figure 2. Cartilage canal thickness in vertebral epiphyseal cartilage.

Heat maps of cartilage canal thickness in the cranial epiphyseal cartilage of: **A**. Five control (heterozygous) and **B**. Five MPS VII dogs. Quantification of: **C**. Overall average cartilage canal thickness; distribution of cartilage canal thickness for **D**. Cranial; **E**. Caudal and **F**. Average (cranial and caudal) epiphyseal cartilage regions. N = 5; bar = 2 mm; median, interquartile range (box), and 10th and 90th percentiles (whiskers).

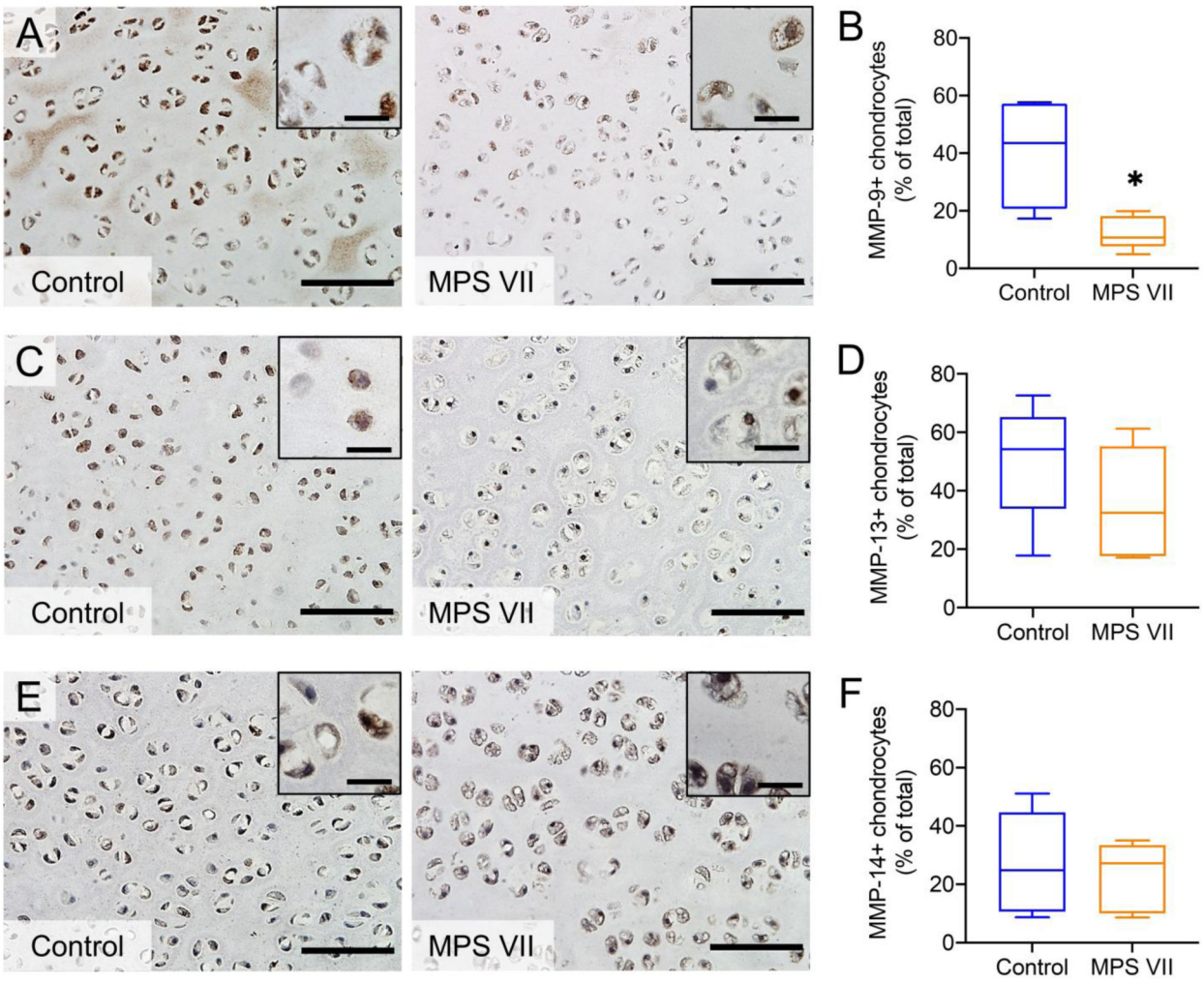

Figure 3. Immunohistochemical assessment of matrix metalloproteinase expression in vertebral epiphyseal cartilage.

Representative staining and quantification of immunopositive cells in control and MPS VII dog epiphyseal cartilage for MMP-9 (**A** and **B**), MMP-13 (**C** and **D**) and MMP-14 (**E** and **F**). Bar = 100 μm (inset scale = 20 μm); n = 5; median, interquartile range (box), and 10th and 90th percentiles (whiskers). *p<0.05, MPS VII vs Control; Mann-Whitney U tests.

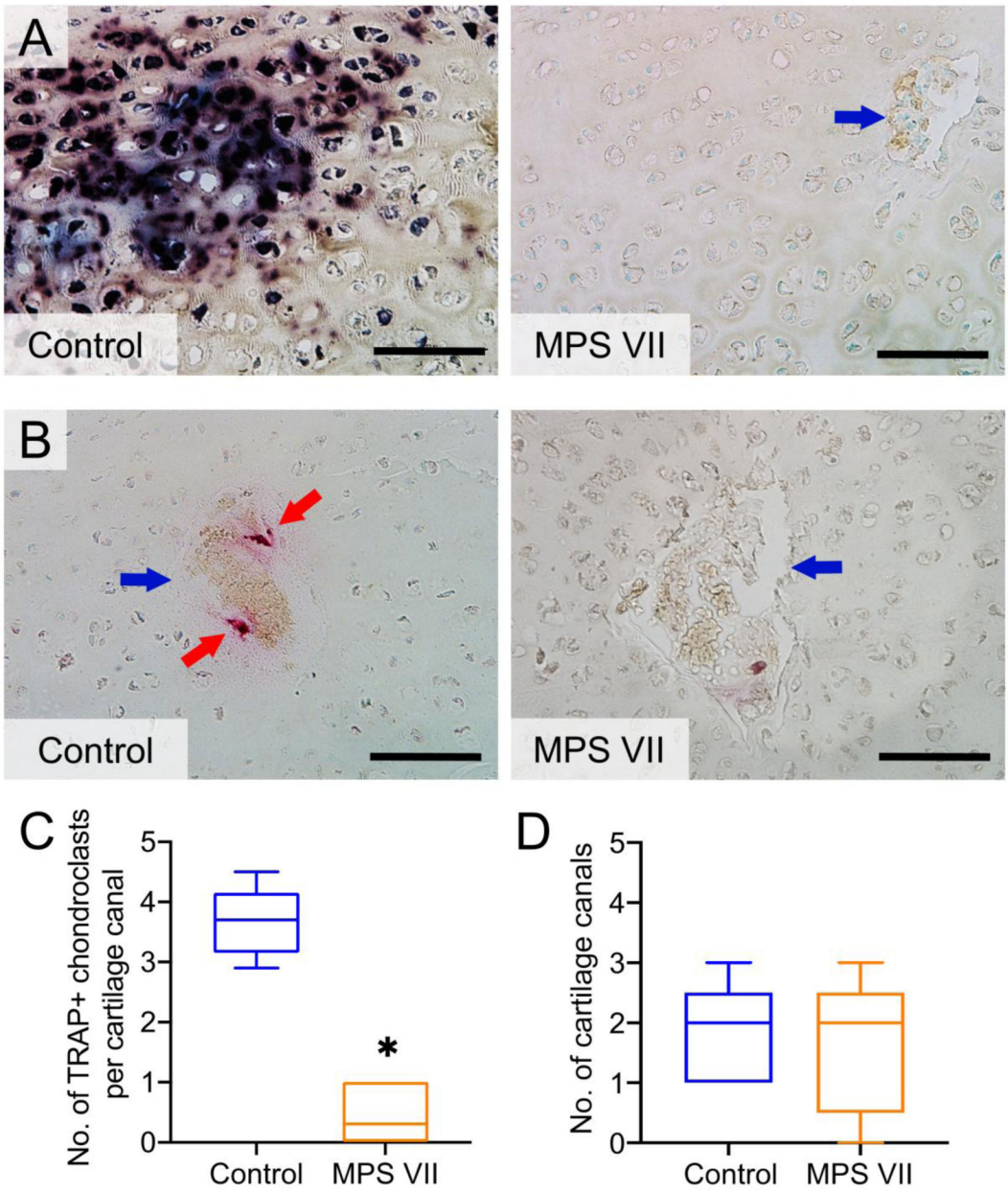

Figure 4. In situ active enzyme staining in vertebral epiphyseal cartilage.

A. Representative ALP staining in control and MPS VII dog vertebral epiphyseal cartilage; **B**. Representative TRAP staining; **C**. Quantification of TRAP-positive chondroclasts; and **D**. Number of cartilage canals in control and MPS VII dog vertebral epiphyseal cartilage. Blue arrows = cartilage canals; red arrows = chondroclasts; bar = 100 μm; n = 5; median, interquartile range (box), and 10^{th} and 90^{th} percentiles (whiskers). *p<0.05, MPS VII vs Control; Mann-Whitney U tests.